

Simulating shot peen forming with eigenstrains

Pierre A. Fauchaux, Frédéric P. Gosselin, Martin Lévesque*

*Département de Génie Mécanique, École Polytechnique de Montréal, CREPEQ, C.P.
6079, Succ. Centre-ville, Montreal, QC H3C 3A7, Canada*

Abstract

Shot peen forming is a cold work process used to shape thin metallic components by bombarding them with small shots at high velocities. Several simulation procedures have been reported in the literature for this process, but their predictive capabilities remain limited as they systematically require some form of calibration or empirical adjustments. We intend to show how procedures based on the concept of eigenstrains, which were initially developed for applications in other fields of residual stress engineering, can be adapted to peen forming and stress-peen forming. These tools prove to be able to reproduce experimental results when the plastic strain field that develop inside a part is known with sufficient accuracy. They are, however, not mature enough to address the forming of panels that are free to deform during peening. For validation purposes, we peen formed several 1 by 1 meter 2024-T3 aluminum alloy panels. These experiments revealed a transition from spherical to cylindrical shapes as the panel thickness is decreased for a given treatment, that we show results from an elastic instability.

Keywords: Peen forming, eigenstrains, 2024 aluminum alloy, elastic instability

1. Introduction

Peen forming is a cold work process predominantly used by aircraft manufacturers to shape wing skins (Baughman, 1970). The process consists of bombarding thin metallic parts with small shots in order to plastically deform a thin surface layer of material. As a result of strain incompatibility be-

*Corresponding author

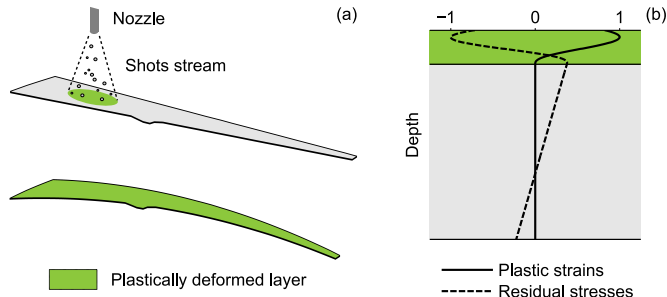


Figure 1: (a) Peen forming of a wing panel. In-plane expansion of the plastically deformed layer causes the part to bend and elongate. (b) Typical (normalized) in plane residual stress and plastic strain profiles after uniform peening. The linear portion in the residual stress profile is due to bending.

tween the surface and the core—left unaffected by the treatment—the whole structure distorts and compressive residual stresses develop near the surface. Figure 1 shows schematically the process application on a wing skin, as well as typical peening-induced plastic strain and residual stress fields. Although the range of accessible curvatures is limited, it is possible to peen form a wide variety of shapes once appropriate parameters are set. Larger curvatures can be achieved by elastically prestraining the parts before peening to increase the effect of the treatment in a given direction (Ramati et al., 1999). This variant of the process is called stress-peen forming.

Simulating the whole process explicitly (i.e., simulating *every* shot hitting the target) is currently beyond reach. For that reason, most available publications on the topic relied on a two-step local-global approach. The local step aims at characterizing the effect of a given treatment on a given material, usually in terms of residual stresses and plastic strains. It is performed either experimentally (Levers and Prior, 1998) or numerically as in the work of Chaise (2011) on ultrasonic shot peening. Mylonas and Labeas (2011) provide an overview of recent research on local peening simulations in a non peen forming-specific context. Stresses or strains induced by the peening treatment are then post-processed to extract loads that are input in structural models of parts to compute equilibrium configurations. The local step involves contact, plasticity, and large deformations that are characteristics of a forming analysis. The global step, on the other hand, can be seen as a springback analysis, as it was demonstrated by Chen et al. (2014) that the re-balancing of the part usually involves only elastic transformations.

Several types of (idealized) loads used in global simulations were reported in the literature: Levers and Prior (1998) and Wang et al. (2006) reproduced the expansion of subsurface layers where Gariépy et al. (2011) used peening-induced non-equilibrated residual stress profiles. The main shortcoming of these approaches is that, although the choice of the loading is guided by some a priori knowledge of the post-peening state, several parameters systematically have to be adjusted by comparing simulated deformed shapes with their experimental counterparts. The workload is significant and simulations are limited to the vicinity of the process parameters for which the calibration has been performed.

We aimed to show that readily available procedures based on the concept of eigenstrain, which are commonly used in other fields of residual stress engineering, can be adapted to simulate peen forming. These tools have the potential to bypass the calibration step and to simulate peening conditions out of reach of existing procedures. To illustrate this point, we investigate the nature of a transition between spherical and cylindrical deformations observed on panels of varying thickness peen formed under identical conditions. The reason behind this transition has not been explained in peening literature yet, to the best of our knowledge.

The paper is structured as follows: section 2 reviews key results and simulation strategies from eigenstrain literature, as well as previous peen forming experimental campaigns. Materials and methods are detailed in section 3. The proposed simulation procedure is presented in section 4. The latter is validated against experimental results from the literature in section 5.1, and against results generated in the course of this study in section 5.2. Both conventional and stress peen forming are considered. The main findings are discussed in section 6.

2. Background

2.1. Eigenstrains

The term eigenstrain, coined by Mura (1987), has been used to designate anelastic deformations inside a structure regardless of the physical phenomenon they originate from. Stress-free strains and inherent strains are equivalent designations sometimes encountered in the literature. The concept of stress-sources (initial unbalanced residual stresses) used by Niku-Lari (1981) for fast experimental estimation of peening induced residual stresses is also intimately related to eigenstrains as both quantities are proportional

(Terasaki et al., 1999). Thermal strains, plastic strains, and volumetric expansion caused by phase transitions or solvent absorption are some examples of eigenstrains. In shot peened parts, only plastic strains usually contribute to the eigenstrains $\boldsymbol{\varepsilon}^*$.

In any structure free of external loads, residual stresses and distortions can always be attributed to an incompatible eigenstrain field. If the latter is known, or if it can be estimated with sufficient accuracy, then the computation of stresses and distortions — the direct problem — can be dealt with as an inclusion problem (Mura, 1987). This approach has been successfully applied to a variety of engineering problems as illustrated by Deng et al. (2007), Hu et al. (2015), and Depouhon et al. (2015) where the authors respectively investigated residual stresses and distortions induced by welding, laser peening and thermo-mechanical treatments. In all of these studies, the authors made use of a two-step procedure involving a local analysis to compute eigenstrains followed by a global springback analysis to obtain the final deformed shape. To map eigenstrains to large scale models, the source of the loading was considered analogous to a thermal expansion. Thermal expansion coefficients $\boldsymbol{\alpha}$ equal to the eigenstrains were defined over the whole domain ($\alpha_{ij} = \varepsilon_{ij}^*$) and a unit increment of temperature was applied. The validity of this procedure stems from the fact that two identical eigenstrain fields yield the same residual stresses and distortions, whatever the physical phenomenon that causes them.

It is commonly accepted that eigenstrains generated by surface treatments are insensitive to the surface’s topography, provided that curvatures vary gradually and that the target is exempt of sharp geometric features (Ah-dad and Desvignes, 1996). This was confirmed experimentally by Coratella et al. (2015) on laser peened Al. 7050 samples. Zhang et al. (2008) also demonstrated that eigenstrains arising in 17-4 PH steel strips shot peened in the conditions of the study were independent of the strips thickness. They suggested that this result might hold for a variety of materials and peening conditions. Similar observations by Achintha and Nowell (2011) on laser peened Ti-6Al-4V support Zhang and collaborators’ hypothesis. These results further suggest that the effect of a given treatment could conveniently be characterized—either numerically or experimentally—in terms of eigenstrains on small representative volumes of the target material. For example, peening a small strip could enable estimating the post-peening state of a massive part subjected to the same sequence of operations, as was already suggested by Niku-Lari (1981).

Since eigenstrains cannot be measured directly, they have to be reconstructed from various experimental data such as elastic strains or residual stresses. It is a complex inverse problem in the general 3D case (Jun et al., 2011), but several robust reconstruction procedures have been developed for specific configurations. They include closed form relations between residual stresses and eigenstrains such as those reported by Ahdad and Desvignes (1996) and Korsunsky (2005), as well as more generic numerical procedures. Korsunsky (2006), for example, started by postulating a form of the eigenstrain field as a sum of trial basis functions, $\boldsymbol{\varepsilon}^* = \sum_{k=1}^N c_k \boldsymbol{\varepsilon}_k^{trial}$. The choice of basis functions was guided by some a priori knowledge of the eigenstrain field shape, and the objective of the procedure was to find coefficients c_k that minimized the squared difference between measured and simulated residual elastic strains. The latter were obtained by successively inputting each basis function in a linearly elastic model of the structure of interest. For a linearly elastic model, the solution to this least-square problem is unique.

2.2. Experimental peen forming results from the literature

2.2.1. Coverage and Almen intensity

The post-peening state of a shot peened part depends on numerous parameters, such as: characteristics of the part itself (material, geometry), properties of the shots (material, size and shape) and process parameters (type of peening machine, type of fixtures used to secure the part, velocity of the shots, angle of impingement, stand-off distance, mass flow rate, peening time and trajectories). As a consequence of the random nature of the process, many of these parameters have to be described by appropriate statistical distributions.

In industrial practice, only two parameters, namely coverage and Almen intensity, are typically used to characterize peening treatments. Coverage is defined as the fraction of the surface covered by dimples if it is smaller than 98 %, and as a multiple of the time necessary to reach full coverage otherwise. (For example, 200 % coverage is obtained by peening a sample twice the time necessary to reach full coverage.) Almen intensity is an indirect measurement of the energy conveyed by the shot stream. It is obtained by peening normalized SAE 1070 steel strips in the same conditions as the part for increasing peening times, and is defined as the deflection of the strips (in unit of length) read at the peening time for which doubling the peening time would cause the deflection to increase by 10 %.

2.2.2. Large scale experimental campaigns

To the best of our knowledge, only Kulkarni et al. (1981) (supported by Boeing) and Villalva-Braga (2011) (supported by Embraer) reported extensive peen forming results in the open literature. Other studies, such as the work of Miao et al. (2010) on aluminum alloy 2024-T3, investigated comparatively fewer peening conditions and were limited to small specimens—predominantly 76×19 mm Almen strip-like geometries.

Kulkarni et al. (1981) peen formed both 2024-T3 and 7075-T6 aluminum alloys rectangular plates. The specimens were 610 mm long, with varying length to width ratios and thicknesses. The influence of shot speed, shot size, coverage, the geometry of the samples and their orientation with respect to the rolling direction were investigated. These results highlight the complex dependence of a specimen’s final curvature on peening conditions. In particular, a transition from spherical shapes (identical curvatures in both longitudinal and transverse directions) to cylindrical shapes (one curvature small compared to the other) as either the shot speed increased or as the length to width ratio approached unity was repeatedly illustrated. The fact that residual stress measurements were not reported hinders the comparison of these results against additional simulations.

Villalva-Braga (2011) peened formed $429 \times 400 \times 50$ mm Al. 7050-T7451 and Al. 7475-T7351 strips, with thicknesses ranging from 2 to 15 mm. Pre-strain in the form of a uniaxial bending was applied to half of the samples while the other half was free to deform. Numerous peening treatments were investigated. These results are further discussed in the following sections where they serve as a benchmark for our simulations. Only peening conditions for which residual stress measurements were available were retained, namely Al. 7050-T7451 strips peened with the treatments listed in table 1. Residual stresses were measured for each peening condition in the longitudinal direction (private communication) by X-ray diffraction on 50×50 mm strips cut from one sample.

3. Experimental methods

3.1. Peening conditions

All peen forming experiments were carried out by Korea Aerospace Industries, an industrial partner. Two peen forming treatments representative of industrial practices were selected, namely: a saturation treatment, and a more intense forming treatment. Table 2 lists the media type, coverage,

Table 1: Peen forming treatments used by Villalva-Braga (2011) for 10 and 15 mm thick plates

Treatment ID	Media [†]	Coverage	Prestrain [‡]	Shots velocity (m/s)
1, 2, 3	S550	200 %	No	16.2, 22.4, 28.6
4, 5, 6	S550	200 %	Yes	16.2, 22.4, 28.6
7, 8, 9	1/8" (steel)	200 %	No	12.5, 16.9, 18.5
10, 11, 12	1/8" (steel)	200 %	Yes	12.5, 16.9, 18.5

[†] S550 and 1/8" shots are 1.4 mm and 3.2 mm in diameter respectively

[‡] Prestrain amplitude depends on the thickness

Table 2: Peen forming treatments used in the experimental campaign

Treatment	Media [†]	Coverage	Almen intensity
Saturation	S230	100 %	16.8 <i>A</i>
Forming	1/8" (steel)	80 %	22.9 <i>C</i>

[†] S230 and 1/8" shots are 0.6 mm and 3.2 mm in diameter respectively

and Almen intensity for these two process conditions. The treatments were applied by the same operator with a portable peening hose. A mass flow rate of 4.3 kg/min, with an approximate stand-off distance of 760 mm, was used for the saturation treatment. A mass flow rate of 8.7 kg/min, with an approximate stand-off distance of 45 mm, was used for the forming treatment. The parts were free to deform during peening.

3.2. Samples

Three kind of samples were peened:

- 1000 × 1000 mm 2024-T3 plates of thickness 5, 10 and 15 mm were used for large scale forming experiments. One plate of each thickness was formed with each treatment (for a total of 6 plates).
- 200 × 50 × 10 mm strips were used to assess process variability. The strips were peened in the same conditions as the plates at 40 %, 60 %, 80 %, and 100 % coverage. Three strips were peened for each condition (for a total of 24 strips).

- $250 \times 250 \times 15$ mm blocks were used for residual stress measurements. For each treatment, one block was peened in the same conditions as the plates (for a total of 2 blocks).

The 5, 10, and 15 mm thick samples were machined from the same 9.53, 12.7, and 19.05 mm thick sheets, respectively. The same amount of material was removed from both sides of the original plates.

3.3. Residual stress measurements

Residual stress profiles were measured by X-ray diffraction at the center of the $250 \times 250 \times 15$ mm blocks by Proto Manufacturing Ltd. on a Proto-LXRD machine equipped with a copper X-ray tube. Diffracting planes $\{311\}$ and a radiocrystallographic constant of 52.94 GPa were selected. A single profile corrected for material removal and stress gradients was generated for each treatment.

3.4. Deformed shapes measurements

Post-peening deformed shapes were acquired by scanning the parts' surface with a coordinate-measuring machine (CMM). The samples were gently held into place with clips during scanning. An 11 by 11 points grid was used for plates whereas strips were scanned along two perpendicular lines passing through the middle of the sample. For strips, measurements were performed on the unpeened side and the position of the probe was recorded every $35 \mu\text{m}$.

The orientation of all the specimens relative to the rolling direction was not recorded. In particular, we had no available information regarding the direction in which residual stress profiles were measured.

4. Peen forming simulation strategy

4.1. Strategy overview

We adopted a conventional local-global approach where eigenstrain profiles were reconstructed from local residual stress measurements, then mapped onto thin-shell structural models to compute final deformed shapes.

The experimental approach was preferred to local impact simulations as identifying a suitable material model for thin rolled aluminum plates subjected to complex, possibly nonproportional loads, represented a significant challenge. In both the reconstruction procedure and global simulations, it

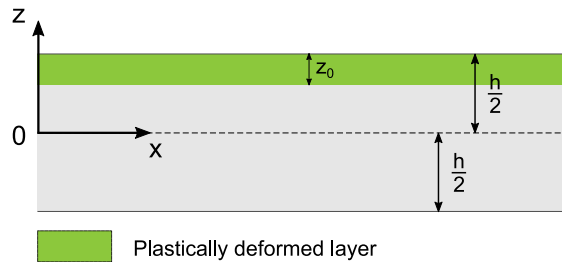


Figure 2: Axis convention

was assumed that strains remained small and that the additive decomposition $\boldsymbol{\varepsilon} = \boldsymbol{\varepsilon}^{el} + \boldsymbol{\varepsilon}^*$ of the total strain $\boldsymbol{\varepsilon}$ between an elastic part $\boldsymbol{\varepsilon}^{el}$ and eigenstrains $\boldsymbol{\varepsilon}^*$ held true. Note that since the only source of eigenstrains in shot peened parts is plastic strains, $\boldsymbol{\varepsilon}^*$ actually corresponds to the plastic part of the strain tensor.

In what follows, the directions along the length and the width of the plates are referred to as x and y respectively, while z denotes the direction normal to the surface. The plate midplane is located at $z = 0$, and the top and bottom surfaces at $z = \frac{h}{2}$ and $z = -\frac{h}{2}$, where h is the plate thickness. These conventions are summarized in Figure 2.

4.2. Local analysis: reconstructing eigenstrain profiles

The eigenstrain fields were reconstructed from limited local residual stress measurements following the inverse procedure reported in Korsunsky (2006).

We assumed eigenstrain profiles of the form $\varepsilon_{xx}^*(z) = \varepsilon_{yy}^*(z) = \sum_{k=1}^N c_k \xi_k(z)$, $\varepsilon_{zz}^*(z) = -2\varepsilon_{xx}^*(z)$ (due to plastic incompressibility) and all other components being equal to zero. This is the form we expect when the target has negligible plastic anisotropy and the coverage is sufficiently high. The ξ_k are basis functions and the c_k are free unknown parameters. Korsunsky's procedure returns the c_k that minimize the error between experimental residual stresses and residual stresses derived from the assumed eigenstrain field. The same basis functions as Korsunsky (2006) were used, namely

$$\xi_k(z) = \begin{cases} \left(\frac{h}{2} - z_0 - z\right)^{k+2} & \text{for } \frac{h}{2} - z_0 \leq z \leq \frac{h}{2}, \\ 0 & \text{otherwise,} \end{cases} \quad (1)$$

where z_0 is the depth of the plastically deformed layer. Since the problem is non-linear in z_0 , Korsunsky (2006) suggested to run the reconstruction procedure several times, each time with a different value for z_0 , and to retain only

the 'best' match. In our implementation, this was done by supplementing the reconstruction procedure by an outer optimization loop over z_0 (performed with Matlab's default *fminsearch* function). The number N of terms in the approximation was set at the beginning of the identification process. It was always taken significantly smaller than the number of experimental points.

Computing the residual stresses for a given eigenstrain profile — the direct problem — requires a model of the structure in which the eigenstrains are inputted. Because of the optimization loop, the direct problem had to be solved numerous times. In order to speed up the process, we used an analytical strength of materials thin plate model identical to that used by Korsunsky (2005). Once a satisfactory value of z_0 was found, the final evaluation of the c_k coefficients was carried out on a 3D finite element model of the samples. This additional step was deemed necessary in order to relax the thin-shell assumption of the analytical plate model used in preliminary runs, as some residual stress measurements were performed on thick samples. All finite element simulations were done with Abaqus 6.14. Meshes of C3D20R brick elements with at least 10 elements over z_0 were used. It should be noted that in all the cases investigated, the values of the coefficients c_k obtained from the analytical model and from the 3D finite element simulations were almost identical.

4.3. Global analysis: computing deformed shapes

4.3.1. Finite element simulations

Since peen forming usually involves large deflections, the models used to compute the deformed shape of peen formed parts must take geometric nonlinearities into account. In what follows, we used off-the-shelf finite element models with large deflection capabilities.

All finite element simulations were done with Abaqus 6.14. The structural models were discretized with regular meshes of multipurpose S4R shell elements checked for convergence. The three translations and the three rotations were set to zero at the central node of the model to prevent rigid body modes. Eigenstrain profiles were input in the finite element models according to the thermal analogy discussed in section 2.1. We used the USDFLD and UEXPAN subroutines to specify the appropriate through-thickness expansion coefficients at each section point. The expansion coefficient values were computed using USDFLD, which can access section point information, and passed as arguments to UEXPAN. Between 10 and 20 section point were used over the thickness z_0 to accurately approximate the eigenstrain profiles.

To ensure that no additional plastic deformation occurred during springback, through-thickness von Mises equivalent stresses were compared to the yield stress of the material at the end of each analysis.

Note that less computer intensive analytical models could have been used for the simple rectangular geometries considered in the next sections. (For example, curvatures can be straightforwardly computed from simple strength of materials models, like that used in section 4.2, when deflections are small).

4.3.2. Loads idealization

Since external loads are integrated over the thickness in conventional thin shell formulations, inputting an idealized profile with the same *resulting* forces and moments as the complete profile yields identical deformed shapes.

For illustration purposes, consider a profile of the form $\varepsilon_{xx}^*(z) = \varepsilon_{yy}^*(z) = \gamma(z)$, ($\varepsilon_{zz}^*(z) = -2\gamma(z)$). We define the resulting eigenstrain $A = \int_{-\frac{h}{2}}^{+\frac{h}{2}} \gamma(z) dz$ and the first eigenstrain moment $B = \int_{-\frac{h}{2}}^{+\frac{h}{2}} \gamma(z) z dz$. These quantities are respectively proportional to the axial force and bending moment per unit length. The simplest idealized profile, which is also the most convenient to input, is a step of amplitude ε_{eq}^* over a depth h_{eq} . For the idealized profile to yield the same resulting loads as the original one, equilibrium requires that $A = h_{eq}\varepsilon_{eq}^*$ and $B = h_{eq}\varepsilon_{eq}^* \left(\frac{h-h_{eq}}{2}\right)$, or $h_{eq} = h - \frac{2B}{A}$ and $\varepsilon_{eq}^* = \frac{A^2}{Ah-2B}$.

A fictitious eigenstrain profile and its idealized counterpart are shown in Figure 3. It can most conveniently be input in any numerical thin plate model by defining a bi-layer laminate section property consisting of an ‘active’ layer of thickness h_{eq} with expansion ε_{eq}^* , and a ‘passive’ layer. The same approach also applies when $\varepsilon_{xx}^*(z) \neq \varepsilon_{yy}^*(z)$: in that case, writing the equilibrium of forces and moments in both x and y directions yields two pair of parameters and the idealized profile can be input by defining a tri-layer stacking sequence with the appropriate expansion in each direction (bi-layer if both directions share the same h_{eq}). Note that, although using an idealized eigenstrain profile yields the same deformed shape as the complete profile, residual stresses will differ. These simplifications are relevant in a peen forming context where the primary concern is to get the shape of the part right and residual stresses are seen merely as a positive side effect.

4.3.3. Dimensional analysis

The final deformed shape of peen formed plates having the same shape, but not necessarily the same thickness, or scale, depends on: a characteris-

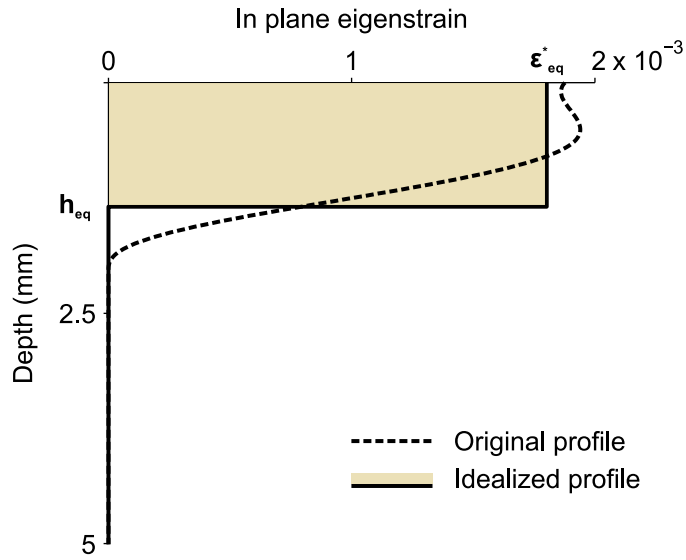


Figure 3: Fictitious eigenstrain profile and idealized profile with equivalent resulting eigenstrain and first eigenstrain moment. The original profile is of the form $\gamma(z) = \sum_{k=1}^4 c_k \xi_k(z)$, with $c_1 = -5.65 \times 10^{-3}$, $c_2 = -6.38 \times 10^{-3}$, $c_3 = -2.48 \times 10^{-3}$ and $c_4 = -3.22 \times 10^{-4}$, with $z_0 = 2.05$ mm. The definition of the basis functions ξ_k is given in section 4.2. The idealized profile is a step of amplitude $\varepsilon_{eq}^* \simeq 1.80 \times 10^{-3}$ over a depth of $h_{eq} \simeq 1.35$ mm. Those two profiles yield the same deformed shapes when input in thin shell models.

tic length of the plate L and its thickness h (geometry), the Poisson ratio ν (material), and, (assuming equi-biaxial expansion of the upper layer) the resulting eigenstrains A and first eigenstrains moment B (loads). It does not depend on Young’s modulus E . Indeed, the modulus is the only quantity that has the dimension of a pressure, thus it cannot be used to form any dimensionless group. This is a consequence of the loads being fully characterized in terms of eigenstrains. Physically, inputting a given eigenstrain profile into a stiff (resp. flexible) material will induce large (resp. small) residual stresses that will be counter-balanced by the plate’s rigidity (both quantities scale with the modulus). Let κ_x be the curvature at the center of the plate along the x axis (resp. κ_y along the y axis). Using this quantity to characterize the deformed shapes, dimensional analysis requires that the problem be fully characterized by 5 dimensionless groups.

We now introduce the dimensionless loads Γ_A and Γ_B , defined respectively as the ratio of in-plane loads over in-plane rigidity, and as the ratio of bending moments over bending rigidity¹. These parameters account for the combined effect of the treatment and the geometry. The former governs in-plane behavior and the latter the bending response. For beams (section 5.1), $\Gamma_A = A/h$ and $\Gamma_B = 12B/h^2$, whereas for thin plates (section 5.2), $\Gamma_A = (1 + \nu)A/h$ and $\Gamma_B = 12(1 + \nu)B/h^2$. The other dimensionless groups we chose were $\kappa_x h$ (resp. $\kappa_y h$), ν , and L/h .

In what follows, all been forming results are presented by plotting $\kappa_x h$ and $\kappa_y h$ as a function of Γ_B after both quantities were rescaled by $\left(\frac{L}{h}\right)^2$. This scaling (obtained by inspection) forces data obtained for different L/h ratios to collapse onto a single master curve.

5. Applications and results

The simulation strategy presented above was validated against experimental results from Villalva-Braga (2011), and against experimental results generated for the purpose of this study. Incomplete data compelled us to

¹The biaxial modulus of a plate is given by $\frac{E}{1-\nu}$ and its bending rigidity by $\frac{Eh^3}{12(1-\nu^2)}$. The axial modulus of a beam is E and its bending modulus $\frac{Eh^3}{12}$. The only loads applied to the system are caused by the eigenstrains. For thin plates whose upper layers expands equibiaxially, $\sigma_{xx}(z) = \sigma_{yy}(z) = \frac{E}{1-\nu^2}(1+\nu)\gamma(z)$, and in-plane loads and bending moments per unit length—obtained after integration over the thickness—are given respectively by $\frac{E}{1-\nu}A$ and $\frac{E}{1-\nu}B$. Similar expressions are obtained for beams by replacing $\frac{E}{1-\nu}$ with E .

make several additional hypotheses on both data sets. These hypotheses are listed before each result section.

5.1. Validation against experimental results from Villalva-Braga (2011)

5.1.1. Working hypotheses

Forming simulations were done according to the procedure presented in section 4. A Young’s modulus of 71 GPa and a Poisson’s coefficient of 0.33 from the MMPDS-08 handbook were used for all simulations.

In Villalva-Braga (2011)’s experiments, prestrain in the form of a uniaxial bending about the y axis was applied to half of the samples. For prestrained plates, as well as for plates that bend significantly, it is expected for ε_{yy}^* to be smaller than ε_{xx}^* (Hu et al., 2015). As a consequence, it was necessary to reconstruct both in-plane components of the eigenstrain field, as both enter the computation of residual stresses (simulated residual stress profiles that the reconstruction procedure attempted to match with measurements depend on the whole eigenstrain field). Since residual stresses measurements in the transverse direction were not available, we assumed an eigenstrain distribution of the form $\varepsilon_{yy}^*(z) = \alpha\varepsilon_{xx}^*(z)$, $0 \leq \alpha \leq 1$. This approximation was expected to yield results close to those observed on slightly bent plates for $\alpha = 1$, whereas taking $\alpha = 0$ yielded an upper bound for ε_{xx}^* .

As Korsunsky’s reconstruction procedure relies on a linearly elastic model of the structure to compute residual stresses, eigenstrain profiles were not extracted from 2 mm thick as well as from some 5 mm thick samples for which the maximum out of plane displacement Δz was not small when compared to the thickness h ($\Delta z > \frac{h}{10}$), and for which geometric nonlinearities might have had to be taken into account.

5.1.2. Results

Table 3 summarizes parameters used to extract eigenstrain profiles on 10 mm thick plates, as well as the characteristics of the idealized profiles used as loads in finite element simulations. The table shows that the depth of the plastically deformed layer z_0 , the depth of the idealized profile h_{eq} , and its amplitude ε_{eq}^* rise as the intensity of the treatment increase. It can also be seen that z_0 et h_{eq} are independent of the choice of α .

Figure 4 displays the eigenstrain profiles extracted for treatments 7 to 9 on free-to-deform 10 mm and 15 mm thick plates. Contrary to the observations of Zhang et al. (2008), it appears that they depend on the plate’s

Table 3: Parameters for the reconstruction of eigenstrain profiles on 10 mm thick plates and characteristics of idealized loadings

Treatment ID	N [†]	z ₀ [†] (mm)	h _{eq} (mm)	ε_{eq}^* ($\times 10^{-3}$)	
				$\alpha = 1$	$\alpha = 0$
1	4	0.76	0.44	2.60	3.46
2	3	0.80	0.54	2.65	3.52
3	4	1.09	0.63	3.29	4.37
4 [‡]	-	-	-	-	-
5	4	1.39	0.76	4.05	5.39
6	5	1.42	0.90	4.09	5.44
7	3	0.95	0.66	3.01	4.00
8	6	1.44	1.09	3.57	4.75
9	6	1.65	1.35	3.91	5.19
10	4	1.50	0.80	4.02	5.34
11	5	2.20	1.23	5.09	6.76
12	7	2.35	1.27	5.03	6.69

[†] Parameters N and z_0 uniquely define the profile for a given set of basis functions and a given set of experimental data.

[‡] Satisfactory reconstruction was not achieved.

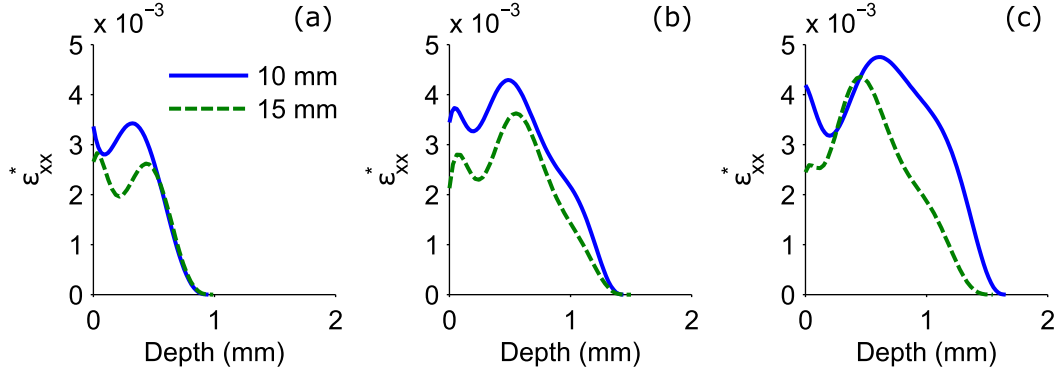


Figure 4: Eigenstrain profiles reconstructed from residual stress measurements of Villalva-Braga (2011) on 10 and 15 millimeter thick plates that were free to deform during peening. It was assumed that $\varepsilon_{xx}^* = \varepsilon_{yy}^*$ ($\alpha = 1$). Treatment number: (a) 7; (b) 8; (c) 9

thickness. It can be seen, however, that from one plate thickness to the next, the profiles have a similar shape and an almost identical z_0 .

Figure 5 compares simulated and experimental curvatures for 10 mm and 15 mm thick plates. Although forming operations were automated, the data exhibits significant scatter. For the thinner samples peened with smaller shots, most experimental points lie within the bounds delimited by simulations. The agreement between simulations and experimental results deteriorates as the treatment intensity increases. For 5 mm thick plates (results not shown here), simulation consistently underestimated experimental curvatures with relative errors ranging from 20 to 75 %, even though a seemingly satisfactory reconstruction of the eigenstrain profiles was achieved. The specific reasons for this behavior are yet to be understood.

Figure 6 shows the same results (for $\alpha = 1$ only) cast into dimensionless form. The results are superimposed to the results of several hundred finite element simulations whose parameters (L , h , h_{eq} , and ε_{eq}^*) were randomly selected from a range of realistic values (ν was kept constant). All numerical results collapse onto a single master curve. Experimental points follow the same trend, except for the outliers identified in Figure 5.

5.2. Peen forming of large 2024-T3 panels

5.2.1. Working hypotheses

Forming simulations were done according to the procedure described in section 4. A Young's modulus of 73.5 GPa and a Poisson's ratio of 0.33 from

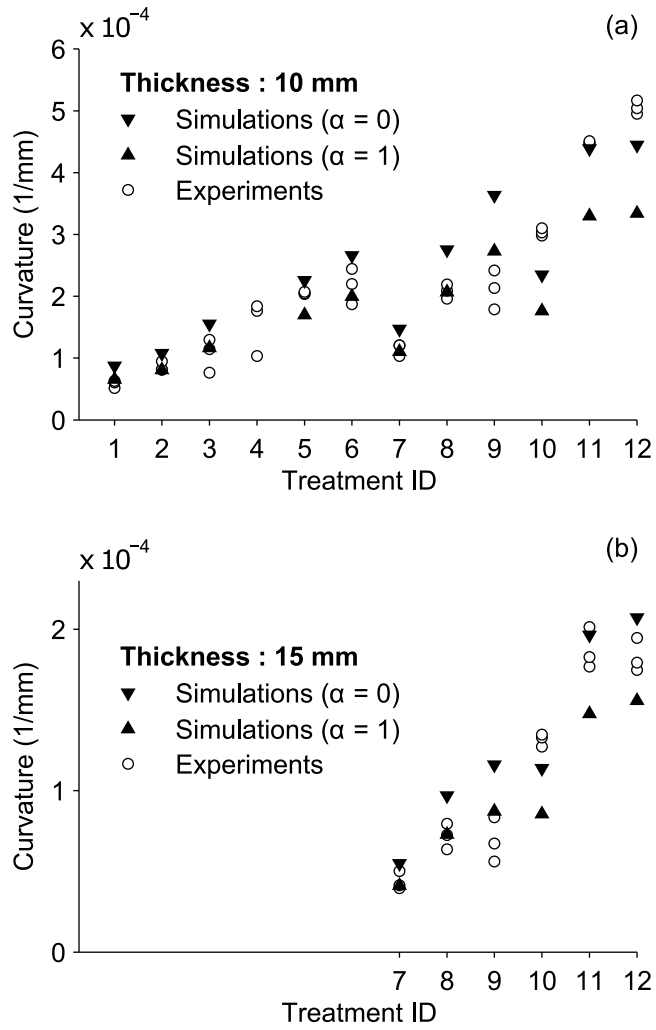


Figure 5: Experimental and simulated curvatures for (a) 10 mm thick and (b) 15 mm thick samples peen formed by Villalva-Braga (2011). Experimental conditions are available in Table 1. Treatments' intensity increases with treatment ID.

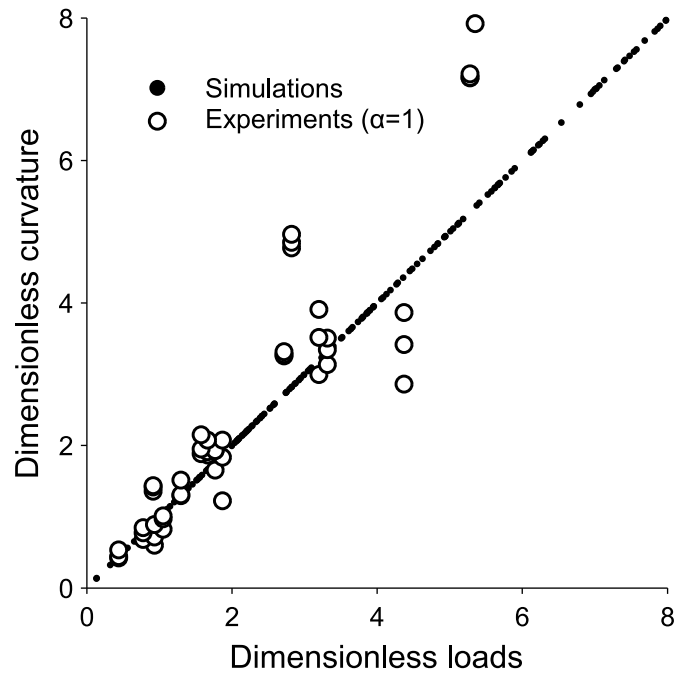


Figure 6: Dimensionless curvature $\kappa_x h \left(\frac{L}{h}\right)^2$ as a function of dimensionless loads $\Gamma_B \left(\frac{L}{h}\right)^2$ for strips of aspect ratio 1 : 8. All parameters for finite element simulations, except ν , were randomly selected from a range of realistic values. Experimental points for $\alpha = 0$ are not shown to avoid clutter. They are slightly offset to the right

the MMPDS-08 handbook were used for all simulations.

Since residual stress measurements were available for the 1000×1000 mm plates, the eigenstrain profiles extracted from the thick $250 \times 250 \times 15$ mm blocks were used as input for all forming simulations. This choice was motivated by the results of Zhang et al. (2008) and Achintha and Nowell (2011) that suggest that peening induced eigenstrain profiles are independent of the part's thickness.

A small imperfection was introduced in the global model to break its symmetry and trigger potential elastic instabilities. These imperfections took the form of a +1 % difference between the amplitude of the expansion input in the model in the x direction (resp. -1 % in the y direction) and ε_{eq}^* . (For actual peen formed parts, such imperfections would be a consequence of material anisotropy, geometric imperfections, boundary conditions and process variability.)

Simulations presented hereafter do not include gravity as running the same simulations considering gravity resulted in variations of curvatures lower than 3 % in all cases.

5.2.2. Results

Figure 7 displays measured residual stress profiles, along with residual stress and plastic strain profiles reconstructed using the procedure of section 4.2, for the $250 \times 250 \times 15$ mm blocks. Figure 7a shows that differences between experimental data and reconstructed residual stress profiles mostly lie within experimental errors, the most significant discrepancy being of 25 MPa. Figure 7b shows that the plastically deformed layer of the forming treatment is about twice as deep as that for the saturation treatment. Although the magnitude of both profiles is similar, residual stresses near the surface are lower for the forming treatment due to the bending of the samples. Table 4 lists the parameters used to extract eigenstrain profiles, as well as characteristics of the idealized profiles used as loads in finite element simulations.

CMM scans of the $200 \times 50 \times 10$ mm strips revealed that curvatures in the transverse direction were always larger than curvatures in the longitudinal direction for this specific geometry, as shown in figure 8. This could be attributed to the known plastic anisotropy of the 2024-T3 aluminum alloy (Bron and Besson, 2004). Indeed, the elastic response of this alloy is almost perfectly isotropic and the curvatures of thick blocks should be identical in both directions if their upper layers expand equi-biaxially.

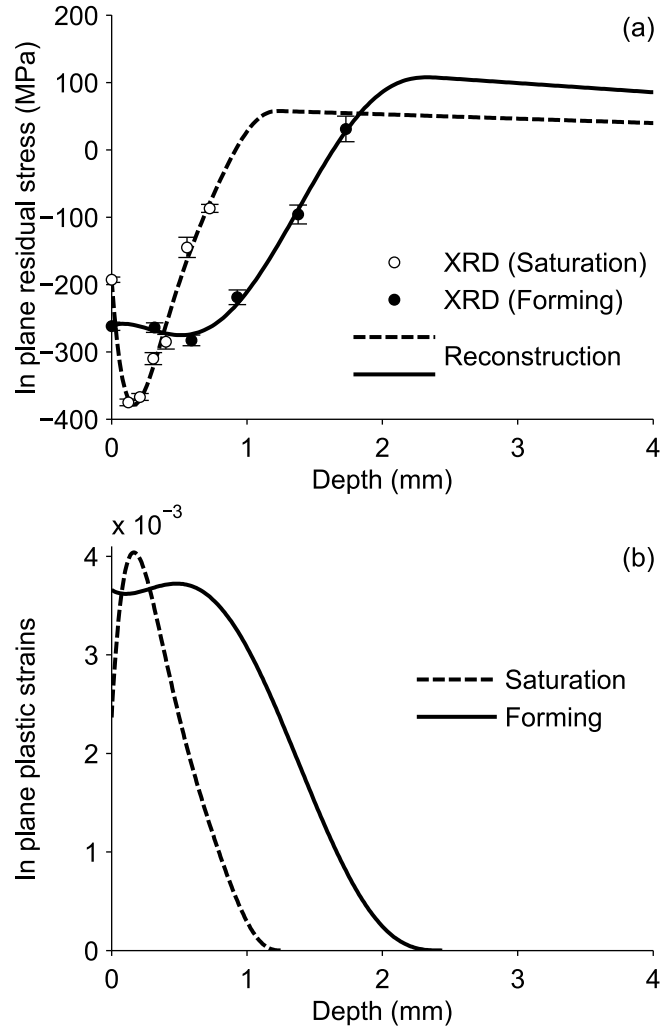


Figure 7: (a) Residual stresses measured by X-ray diffraction on $250 \times 250 \times 15$ mm blocks of 2024-T3 superimposed onto the residual stress profiles derived from the eigenstrain fields from Figure 7.b. (b) Eigenstrain profiles reconstructed with Korsunsky (2006) procedure. The parameters used for the reconstruction are reported in table 4

Table 4: Parameters for the reconstruction of eigenstrain profiles and characteristics of idealized loadings

Treatment	N	z_0 (mm)	h_{eq} (mm)	ε_{eq}^* ($\times 10^{-3}$)
Saturation	4	1.26	0.72	3.22
Forming	3	2.44	1.51	3.42

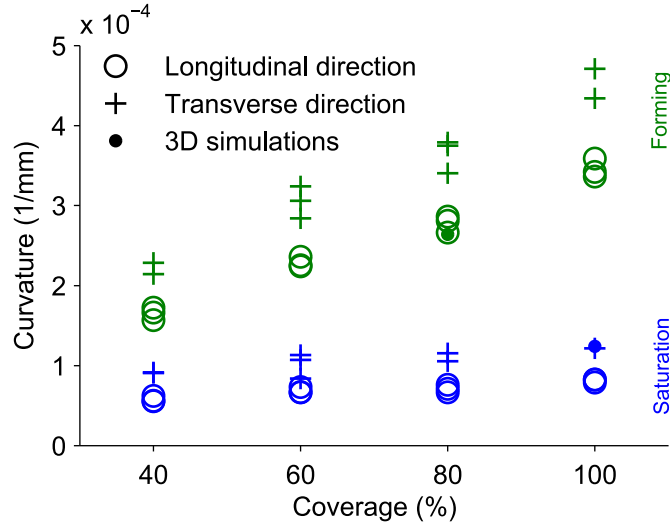


Figure 8: Measured curvatures as a function of coverage along longitudinal and transverse directions on $200 \times 50 \times 10$ mm strips for both saturation and forming treatments. Simulated curvatures obtained by inputting the eigenstrain profiles from Figure 7 in a 3D finite element model of the strips are also reported. For the simulations, curvatures in both directions are equal

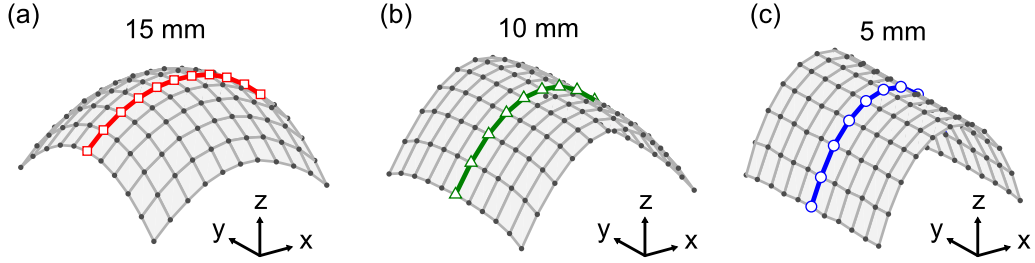


Figure 9: Measured deformed shapes (not to scale) of 1×1 m 2024-T3 plates of thickness (a) 15 mm, (b) 10 mm and (c) 5 mm subjected to the forming treatment. The plates were free to deform during peening. Interpolation of the surface between experimental points is here only to guide the eye. Similar shapes were observed for the saturation treatment.

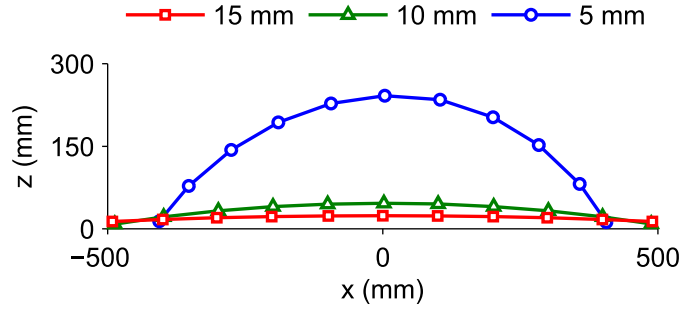


Figure 10: Cross sectional views in the (xz) plane passing through the center of the plates of the results of Figure 9.

CMM scans of the 1000×1000 mm plates revealed that thick shot-peened plates consistently adopted an hemi-spherical shape, whereas thinner plates deformed cylindrically. This is illustrated in Figure 9 for the forming treatment. The magnitude of the out-of-plane deflection varied significantly between those two configurations, as shown in Figure 10. Curvatures at the center of the plate along the x and y axes are given in Table 5. It should be noted that the curvatures were always approximately constant over the scanning lines, with the exception of slight variations near the edges.

Table 5 compares simulated curvatures against validation experiments. The table reveals that simulations successfully captured the overall deformed shapes (i.e., spherical or cylindrical). Quantitative agreement is only satisfactory for the 15 mm thick plate submitted to the forming treatment (note that the eigenstrain profile was extracted from a sample of the same thick-

Table 5: Experimentally measured and simulated curvatures for 1000×1000 mm 2024-T3 plates.

Treatment	Thickness (mm)	Experiments (1/mm)		Simulations (1/mm)		Relative error (%)	
		κ_x	κ_y	κ_x	κ_y	Along x	Along y
Saturation	5	4.25×10^{-4}	$\simeq 0$	5.82×10^{-4}	$\simeq 0$	37	-
Saturation	10	5.86×10^{-5}	5.55×10^{-5}	8.71×10^{-5}	7.13×10^{-5}	49	28
Saturation	15	3.15×10^{-5}	2.84×10^{-5}	5.53×10^{-5}	5.26×10^{-5}	76	85
Forming	5	2.17×10^{-3}	$\simeq 0$	1.10×10^{-3}	$\simeq 0$	-49	-
Forming	10	3.08×10^{-4}	$\simeq 0$	2.63×10^{-4}	$\simeq 0$	-15	-
Forming	15	9.93×10^{-5}	7.91×10^{-5}	9.71×10^{-5}	8.91×10^{-5}	-2	13

ness). Curvatures were largely underestimated for thinner plates for the forming treatment. They were overestimated in all cases for the saturation treatment.

Figure 11 presents the results of Table 5 cast into dimensionless form. They are superimposed to the results of several hundred finite element simulations whose parameters (except ν , which was kept constant) were randomly selected from a range of realistic values. Finite element simulations reveal that, for small dimensionless loads, curvatures are identical in both principal directions, yielding a spherical shape. As dimensionless loads increase, one of the curvatures drops to zero while the other increases steadily, yielding a cylindrical shape. Between those two extremes, simulations predict a narrow region where curvatures assume distinct but nonzero values. Such elliptic shapes can indeed be observed in Figure 9.b.

6. Discussion

The procedure presented in this article differs from existing peen forming simulations in that the link between the loads used in global simulations and the post-peening state is now explicit, thus bypassing the need for lengthy calibration phases. This was made possible by determining the plastic strain field for each combination of material, treatment and prestrain. The procedure is otherwise similar to those reported by Levers and Prior (1998) and Wang et al. (2006), and is almost identical to the procedure reported in Gariépy et al. (2011). Indeed, induced stresses used as loads by Gariépy et al.—defined as ‘unbalanced residual stresses [...] encountered in a fully constrained component that does not allow stretching or bending’—are directly proportional to eigenstrains (Korsunsky, 2005).

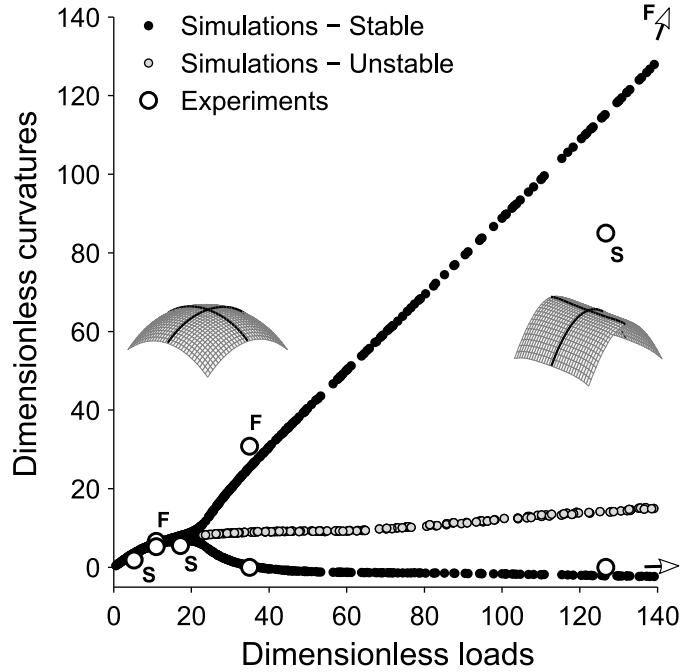


Figure 11: Dimensionless curvatures $\kappa_x h \left(\frac{L}{h}\right)^2$ and $\kappa_y h \left(\frac{L}{h}\right)^2$ as a function of dimensionless loads $\Gamma_B \left(\frac{L}{h}\right)^2$ for square panels. The tags **F** and **S** refer to the forming and to the saturation treatments respectively. Results for the 5 mm plate subjected to the forming treatment lie outside the graph at (230, 0) and (230, 434). All parameters for finite element simulations, except ν , were randomly selected from a range of realistic values. For dimensionless loads smaller than $\simeq 22$, there is a single spherical equilibrium shape. For larger values of this parameter, two cylindrical configurations (bending along x or bending along y) and one instable spherical configurations coexist. A small imperfection was input in the model to trigger the transition from the unstable spherical to a stable cylindrical shape.

The results of section 5.1 revealed that the proposed procedure yielded excellent agreement between simulated and experimental curvatures for moderate intensity treatments, both for free-to-deform and stress peen formed (i.e. prestrained) parts, provided that the post peening state was accurately known. For large shots, experimental results lay outside the bounds delimited by simulations. Recall that those bounds were obtained for limiting cases (namely uniaxial and equi-biaxial plastic strains). Identifying the reason behind these discrepancies is yet to be done. Obtaining more experimental data could provide more insight. In particular, some characterization of the response in the transverse direction would have been desirable.

In Section 5.2, the same procedure was applied to predict the deformed shape of free-to-deform plates based on residual stress measurements performed on thick blocks of material. Recall that these simulations were carried out under the assumption that shot-peening-induced plastic strains were independent of the part's thickness. This approach significantly underestimated the curvature of free-to-deform thin panels subjected to the forming treatment. The eigenstrain profiles reported in Figure 4 suggest that this difference could be attributed to the stress peen forming that takes place as the plates deform: thinner plates exhibit larger curvatures, larger prestrains and hence larger subsurface expansion than those measured on thicker plates. Unlike the stress-peen forming experiments of Villalva-Braga (2011), the pre-strain was a consequence of the continuous re-balancing of the part. Not only was it complex and continuously evolving as the treatment progressed, it was also path dependent. For this kind of simulations, the local and global models would have to be coupled, as was already concluded by Cao et al. (1995) and Gariépy et al. (2011). The coupling was not accounted for in this article. The main impediment in simulating free-to-deform panels is the availability of models able to produce fast estimates of the post-peening state, possibly for partial coverages, for each increment of the simulation. Identifying a suitable material model for the aluminum alloys that are used to manufacture the vast majority of peen formed parts is another (plastic anisotropy, cyclic non-proportional loading and experimental identification on thin sheets). We recognize that simplified procedures could be developed for special cases as was done by Cao et al. (1995) for parts treated until saturation (i.e. for which an increase in peening time does not result in additional deflection).

These elements do not explain why the curvatures induced by the saturation treatment were overestimated. One possible explanation is that the simulations did not account for the 2024-T3 aluminum alloy's plastic anisotropy.

This plastic anisotropy could lead to direction-dependent plastic strains. If the only residual stress profile available for the saturation treatment—which was then used to feed the forming simulations—was measured in the direction along which the magnitude of plastic deformations was the largest, it is likely that simulated curvatures were over-estimated. This supposes that the contribution of continuous re-balancing (if there is one) was small compared to the contribution of plastic anisotropy, which is possible since plates peened with the saturation treatment were only slightly bent (the out of plane deflection of the 5 mm thick plate formed with the saturation treatment is 63 mm). Additional residual stress measurements would be necessary to confirm this hypothesis. Variability in the process could also play a role. Indeed, the process is intrinsically random and some dispersion is unavoidable, as illustrated in Figures 5 and 8 (note that every sample was peened under the same conditions and that the results of Villalva-Braga (2011) were generated on an automated peening setup). Here, we tacitly assumed that the only residual stress profiles available were representative of the average post-peening state. It is to be expected that the effect of this dispersion would be less pronounced for thicker plates, as finite element simulations of Figure 11 predict that variations in subsurface expansion do not affect curvatures as significantly as they do for thinner plates (the sensibility of curvature with respect to the ‘intensity’ of the treatment for a given geometry, which corresponds to the slope of the curve, is approximately twice as low before the bifurcation than it is after).

Although it failed at making quantitative predictions in a number a situations, the proposed model captured the main features of the response of peened formed plates, in particular the transition from spherical to cylindrical shapes evidenced in Figures 9, 11, and by Kulkarni et al. (1981). Neglected by the peening community, similar phenomenon (i.e. the shape transition of a thin plate whose upper layers expand/contract) have been extensively studied in the context of composites (Hyer, 1981) and MEMS manufacturing (Freund and Suresh, 2004). Even though the physical sources of eigenstrains may differ, the model system used in those publications is identical to that presented here (a thin multilayer plate with prescribed strain mismatch). By thinking in terms of eigenstrains, it is possible to transpose the conclusion that the transition results from an elastic instability to our specific problem. Insight into the physics of the transition can be gained by considering the following argument (see Pezzulla et al. (2016) and Freund and Suresh (2004) for a more in depth analysis): for a thin plate, the elastic energy of a cylindri-

cal shape (pure bending without extension of the neutral axis) varies with h^3 whereas the elastic energy of a spherical shape (purely in extension as spheres are non-developable surfaces) varies with h . Since the plate seeks to adopt the shape with minimal energy, the sphere is favored for large thicknesses and vice-versa. The bifurcation occurs when the two energies are comparable. Past the bifurcation point, the spherical shape remains an equilibrium configuration but it is unstable (Fig. 11). Note that in Figure 11, the progressive nature of the transition is a consequence of the small imperfections input in the model.

Figure 11 also demonstrated that with a proper choice of dimensionless parameters, the results of all simulations, as well as most experiments, collapsed onto a single master curve. Similar curves can readily be obtained for random geometries, as illustrated in Figure 6 for rectangular strips of aspect ratio 1 : 8. They enable fast appreciation of the influence of the treatment, thickness and scale, and could prove most useful to support fast engineering decisions in developing peen forming strategies. One could also envision adjusting peening parameters and peening patterns on scale models of complex parts before scaling up to production. This would be of particular interest to industrials as discussed in Kulkarni et al. (1981). Scaling relations derived from the results of Section 4.3.3 are given in the appendix for information.

7. Conclusion

In this article, we demonstrated that a decoupled local-global simulation procedure based on the concept of eigenstrains can predict, without calibration, the deformed shape of peen formed plates, provided that the post-peening state of the material is known, or that it can be predicted with sufficient accuracy. The same procedure was used to predict the shape of large free-to-deform thin panels based on eigenstrain profiles obtained on small thick samples. This approach proved to be inadequate when the parts bent significantly during the peening treatment, i.e. when the local and global scales were strongly coupled.

A selection of peen forming experiments on large 2024-T3 aluminum alloy plates was also presented. These results highlighted a transition from spherical to cylindrical deformed shapes as the thickness of the panels decreased for a given treatment. By reasoning in terms of eigenstrains, it was possible to reuse existing results from studies in the fields of MEMS and composite manufacturing to show that this transition was caused by an elastic instability.

This information could enable industrials to develop new forming strategies making use of instabilities instead of trying to avoid them (Baughman, 1970).

We believe that this kind of approach (i.e. reduction to previously solved problems) has the potential to quickly widen the range of tools available for the simulation of peen forming. Such tools are essentials for peen forming to get rid of its black-art reputation.

8. Acknowledgements

The authors gratefully acknowledge financial support from Airbus, the Rio Tinto group through a graduate scholarship, as well as the Canada Research Chairs program.

Appendix A. Scaling relations for geometrically similar peen formed parts

Consider two geometrically similar plate-like structures, one of which has been peen formed to the desired target shape, and the other one being a scale model whose dimensions have been scaled by a factor c . Subscripts 1 and 2 are used to distinguish between the two systems.

If only equi-biaxial in plane eigenstrains develop inside the parts, their deformed shape is entirely characterized by the couple of dimensionless parameters $\{\Gamma_{Ai}, \Gamma_{Bi}\}$, $i = 1, 2$. For the two parts to adopt the same deformed shape, the two systems must have identical Γ_{Ai} and Γ_{Bi} . If both parts have the same Poisson ratio, this yields $A_2 = c A_1$ and $B_2 = c^2 B_1$, or alternatively, $h_{eq2} = c h_{eq1}$ and $\varepsilon_{eq2}^* = \varepsilon_{eq1}^*$.

References

- Achintha, M., Nowell, D., Jun. 2011. Eigenstrain modelling of residual stresses generated by laser shock peening. *Journal of Materials Processing Technology* 211 (6), 1091–1101.
- Ahdad, F., Desvignes, M., 1996. Contraintes résiduelles et déformations plastiques. Leurs relations mutuelles pour des pièces de géométries simples. *Matériaux et techniques* 84 (5-6), 46–50.
- Baughman, D. L., 1970. Peen forming. *Machine design* 42 (27), 156–160.

- Bron, F., Besson, J., Apr. 2004. A yield function for anisotropic materials Application to aluminum alloys. *International Journal of Plasticity* 20 (4-5), 937–963.
- Cao, W., Fathallah, R., Castex, L., 1995. Correlation of Almen arc height with residual stresses in shot peening process. *Materials science and Technology* 11 (9), 967–973.
- Chaise, T., 2011. Mechanical simulation using a semi analytical method: from elasto-plastic rolling contact to multiple impacts. Ph.D. thesis, INSA de Lyon.
- Chen, Z., Yang, F., Meguid, S. A., 2014. Realistic finite element simulations of arc-height development in shot-peened almen strips. *Journal of Engineering Materials and Technology* 136 (4), 041002.
- Coratella, S., Sticchi, M., Toparli, M., Fitzpatrick, M., Kashaev, N., Jul. 2015. Application of the eigenstrain approach to predict the residual stress distribution in laser shock peened AA7050-T7451 samples. *Surface and Coatings Technology* 273, 39–49.
- Deng, D., Murakawa, H., Liang, W., Sep. 2007. Numerical simulation of welding distortion in large structures. *Computer Methods in Applied Mechanics and Engineering* 196 (45-48), 4613–4627.
- Depouhon, P., Sprauel, J., Mermoz, E., 2015. Prediction of residual stresses and distortions induced by nitriding of complex 3d industrial parts. *CIRP Annals - Manufacturing Technology* 64 (1), 553–556.
- Freund, L. B., Suresh, S., 2004. *Thin film materials: stress, defect formation and surface evolution*. Cambridge University Press.
- Gariépy, A., Larose, S., Perron, C., Lévesque, M., Oct. 2011. Shot peening and peen forming finite element modelling – Towards a quantitative method. *International Journal of Solids and Structures* 48 (20), 2859–2877.
- Hu, Y., Li, Z., Yu, X., Yao, Z., Jul. 2015. Effect of elastic prestress on the laser peen forming of aluminum alloy 2024-T351: Experiments and eigenstrain-based modeling. *Journal of Materials Processing Technology* 221, 214–224.

- Hyer, M. W., 1981. Calculations of the room-temperature shapes of unsymmetric laminates. *Journal of Composite Materials* 15, 296–310.
- Jun, T.-S., Venter, A., Korsunsky, A., Feb. 2011. Inverse Eigenstrain Analysis of the Effect of Non-uniform Sample Shape on the Residual Stress Due to Shot Peening. *Experimental Mechanics* 51 (2), 165–174.
- Korsunsky, A. M., Apr. 2005. On the modelling of residual stresses due to surface peening using eigenstrain distributions. *The Journal of Strain Analysis for Engineering Design* 40 (8), 817–824.
- Korsunsky, A. M., Apr. 2006. Residual elastic strain due to laser shock peening: modelling by eigenstrain distribution. *The Journal of Strain Analysis for Engineering Design* 41 (3), 195–204.
- Kulkarni, K. M., Schey, J. A., Badger, D. V., 1981. Investigation of shot peening as a forming process for aircraft wing skins. *Journal of Applied Metalworking* 1 (4), 34–44.
- Levers, A., Prior, A., 1998. Finite element analysis of shot peening. *Journal of Materials Processing Technology* 80, 304–308.
- Miao, H., Demers, D., Larose, S., Perron, C., Lévesque, M., Nov. 2010. Experimental study of shot peening and stress peen forming. *Journal of Materials Processing Technology* 210 (15), 2089–2102.
- Mura, T., 1987. *Micromechanics of Defects in Solids*, 2nd Edition. No. 3 in *Mechanics of Elastic and Inelastic Solids*. Springer Netherlands.
- Mylonas, G., Labeas, G., Jun. 2011. Numerical modelling of shot peening process and corresponding products: Residual stress, surface roughness and cold work prediction. *Surface and Coatings Technology* 205 (19), 4480–4494.
- Niku-Lari, A., 1981. Méthode de la flèche. Méthode de la source des contraintes résiduelles. In: *Proc. 1st Conf. Shot Peening (ICSP1)*. Paris, France, pp. 237–247.
- Pezzulla, M., Smith, G. P., Nardinocchi, P., Holmes, D. P., 2016. Geometry and mechanics of thin growing bilayers. *Soft Matter* 12 (19), 4435–4442.

- Ramati, S., Levasseur, G., Kennerknecht, S., 1999. Single piece wing skin utilization via advanced peen forming technology. In: Proc. 7th Conf. Shot Peening (ICSP7). Warsaw, Poland.
- Terasaki, T., Chen, J., Akiyama, T., Kishitake, K., 1999. Non-destructive method for estimating residual stress distribution in component due to shot peening. *JSME International Journal Journal Series A Solid Mechanics and Material Engineering* 42 (2), 216–223.
- Villalva-Braga, A. P., 2011. Análise de ligas de alumínio aeronáuticas conformadas por jateamento com granalhas-caracterização e previsão de deformação. Ph.D. thesis, Universidade de São Paulo.
- Wang, T., Platts, M., Levers, A., Feb. 2006. A process model for shot peen forming. *Journal of Materials Processing Technology* 172 (2), 159–162.
- Zhang, S. Y., Venter, A., Vorster, W. J. J., Korsunsky, A. M., Apr. 2008. High-energy synchrotron X-ray analysis of residual plastic strains induced in shot-peened steel plates. *The Journal of Strain Analysis for Engineering Design* 43 (4), 229–241.